Numerical simulation of the sorption phenomena during the transport of VOCs inside a capillary GC column

Alberto Rodríguez Cuevas, Ricardo Brancher, Frédéric Topin, Stéphane Le Calvé, Irina Graur

Numerical simulation of the sorption phenomena during the transport of VOCs inside a capillary GC column

Alberto Rodriguez-Cuevas[1,2], Ricardo D. Brancher[2,3], Fréderic Topin[2], Stéphane Le Calvé[1,4], Irina Graur[2]

[1] *In'Air Solutions, 25 rue Becquerel, 67087 Strasbourg, France*

[2] *Aix-Marseille Université, CNRS, IUSTI UMR 7343, 5 rue E. Fermi, 13453, Marseille, France*

[3] *Institute of Mechanics, BASci., Acad. G. Bonchev Str., Block. 4, 1113, Sofia, Bulgaria*

[4] *Université de Strasbourg, CNRS, ICPEES UMR 7515, F-67000 Strasbourg, France*

Abstract

A mathematical model based on Langmuir kinetic approach is proposed to describe the transport of BTEX molecules (benzene, toluene, ethylbenzene, m-, p- and o-xylene) inside a capillary chromatography column during their separation step. This model is numerically implemented and afterwards it is validated in correlation with experimental data. Since some thermodynamic parameters and chemical coefficients are unknown for our surface kinetics the initial adsorption and desorption coefficients, K_{ads} and K_{des}, are derived from the experimental data. Afterwards predictions are achieved with a good level of correlation when calculating the retention time and peak width at the column outlet for an experimental sequence of several different column temperatures and inlet pressures; and comparing these values with the equivalent simulations.

1. Introduction

When two different solutes α and β flow through a Gas Chromatography (GC) column carried by a carrier gas, they can interact differently with the stationary phase. If species α is more strongly adsorbed on the stationary phase than the species β, this means its displacement along the column is slower,

Email addresses: alberto.rodriguezc@alumnos.unican.es (Alberto Rodriguez-Cuevas[1,2]), Ricardo.d.brancher@gmail.com (Ricardo D. Brancher[2,3]), frederic.topin@univ-amu.fr (Fréderic Topin[2]), slecalve@unistra.fr (Stéphane Le Calvé[1,4]), irina.martin@univ-amu.fr (Irina Graur[2])

consequently, this species α will spend more time to reach the outlet of the column than the species β [1].

There are two main factors which indicate how well the compounds are separated inside the column: the retention time (RT) and the width of the peaks (WOP). The RT is a measure of the time taken for a solute to pass through a chromatography column. It is calculated as the time from injection to detection, which corresponds, in the absence of significant dead volumes between the injector, the column and the detector, to the time spent in the column. The difference in the RT of the species is crucial in the chromatographic process. If the values of retention time of two species are too similar, the separation will not be clear and therefore the identification of each analyte will not be possible.

The quality of analysis is also related to the WOP the narrower and taller the peaks the better. If the peaks of two species are too wide, they can overlap each other making it difficult to obtain accurate measurement of the area under the peaks, usually called peak area integration. Thus, it is indispensable that the peaks are separated from each other. Nonetheless, the RT and the width of the peak for a compound are not fixed as many factors can influence them even if the same GC system and column are used. These factors include carrier gas flow rate, temperature differences, varying from one analysis to another, or column degradation.

In the ideal case, the columns should be very long and narrow, while the retention times of the different analytes should be different enough to have fully independent peaks. However, in the reality the concentration of a solute moving through a chromatography column tends to spread into a Gaussian shape [1]. The longer the solute resides in the column, the wider the Gaussian peak becomes. Therefore, once satisfied the condition that the peaks should not overlap, it is desirable that the retention times are as short as possible, in order to decrease the time consumed by the separation. Aiming to obtain a chromatogram close to the ideal one, it is critical to select the optimal operating conditions, that is, the best parameters such as stationary phase, carrier gas, pressure difference, and temperature, among others.

In actual practice, when there is a necessity to acquire a new gas chromatography column, to separate one or more families of VOCs, the choice is based on some general guidelines and previous experience from the experts working in the field [2]. The selection of the stationary phase polarity, its thickness, inner diameter and length of the column are often done upon some generic approximations and concepts. For example, in many occasion, the choice of the stationary phase composition is done using the concept "equal dissolve equal". Consequently, often the best column option is not the one eventually selected. Generally, the variables influencing the performance of the chromatographic process are so abundant that selecting a good chromatography column is indeed a very difficult task. The best choice of the parameters like temperature, use of isothermal condition, temperature ramps, inlet and outlet pressures, volume and duration of the injection, optimal velocity of the gas through the column or carrier gas type require a huge amount of systematic experiments. This means a lot of time, resources and efforts.

The objective of the work presented here is to develop a mathematical model and implement it in a numerical code to predict the behavior of the BTEX molecules separation inside a chromatographic column. It should be clarified that the objective here is not to create a complete program taking into account all the above-mentioned parameters, but developing a numerical code considering some of these parameters, which could be used as the first step in the process of choosing a column, namely, temperature, pressure, concentration of the species, properties of the carrier gas, length and radius of the GC column. Other parameters such as flow distortions due to the injections will not be considered. Moreover, the model will be evaluated in 1D following the column length, to reduce the computational cost, but considering the radial fluxes through integration over the column cross-section.

Several authors have developed alternative models to estimate retention times of aromatic molecules inside GC-columns [3], [4], [5], [6], [7]. This approach could be applied to the transport of various molecules flowing through a GC column. Among all the pollutants detected by using gas chromatography, the BTEX compounds (benzene, toluene, ethylbenzene, o-xylene, p-xylene and m-xylene) are the ones used as a reference in the present study to create and validate our numerical model. The harmful effects of this family of volatile organic compounds (VOCs) are well documented [8], [9] and several groups and companies are developing gas analyzers to detect them more accurately in the indoor environment [10], [11]. In light of the efforts being done to develop more and more accurate sensing systems [12], [13], proper VOCs separation is highly needed to quantify even the smallest concentrations of each individual species. The chemical family studied in these articles is a good example of this necessity. The BTEX compounds have very similar chemical properties however the impact on human health varies a lot from one specie to the other. Benzene is a well-known carcinogenic when chronicle exposure at ppb levels while xylene only generate irritation in sharp exposures over dozens of ppm. Thus, a correct separation and identification is critical.

Table 1 presents some important physical and chemical characteristics of the BTEX compounds, while Figure 1 shows the chemical structure of the BTEX molecules.

Molecule	Benzene	Toluene	Ethylbenz.	p-Xylene	m-Xylene	o-Xylene	Nitrogen
molecular weight ($\mathcal{M}$)[g/mol]	78.11	92.14	106.17	106.16	106.16	106.16	20.01
Molecular mass (m) $\times 10^{27}[kg]$	129.71	153.00	176.30	176.29	176.29	176.29	46.52
Molecular diameter (d) $\times 10^{10}[m]$	5.26	5.68	6.02	6.80	6.80	6.80	4.17

Table 1: Physical and chemical parameters of BTEX and N_2.

We propose a new methodology for the modeling of the properties of gas transport in the chromatography column, including advection and diffusion mechanisms, and also considering the adsorption and desorption on the stationary phase. This approach could be applied to the transport of various molecules flowing through a GC column even if we implement it to a particular column for the BTEX molecules analysis. In addition, the adsorption-desorption mech-

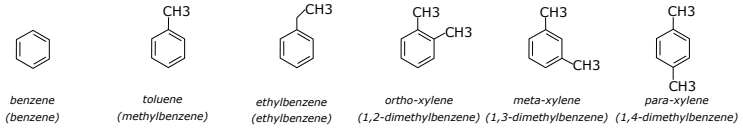

Figure 1: Molecular structure of all the BTEX compounds.

anism could be also used for the pollutant detection, not only by CG column, but also by the microfluidics biosensors, see for example Ref. [14].

This article is organized as following. First, the mathematical model is proposed to describe the interaction (in terms of adsorption-desorption) between the stationary phase and each of the analytes in the GC column in combination with the effects of the transport of the molecules by the carrier gas and diffusion. Afterwards, the proposed model is applied to simulate the behavior of the BTEX molecules in the chromatography column with PDMS as the stationary phase. Finally, to check the accuracy of the proposed model, the comparison between experimental data and the numerical results is presented.

2. Mathematical model

We start by a short description of the adsorption-desorption model used for the simulation of the interaction between the pollution species and the stationary phase. Then, we present the model of single gas transport through a long tube generated by the pressure difference applied at the tube ends. Finally, the diffusion and advection effects are quantified and the interaction between the mobile phase and stationary phase, in terms of the adsorption and desorption processes, are discussed.

2.1. Model of adsorption and desorption

Adsorption is the adhesion of atoms, ions or molecules from a gas, liquid or dissolved solid to a surface [15], [16]. This process creates a film of the adsorbate on the surface of the adsorbent. Adsorption is often brought on by ion exchange, that causes the mobile tracer to adhere to the surface and thus it becomes immobile.

In the simplest case, the adsorption process can be envisioned as a reversible chemical reaction where one adsorption site on the solid reacts with a molecule to produce an absorbed molecule. To describe the adsorption and desorption processes we denote $N(t, x)$ the amount of adsorbed solute. Since the molecules become attached to solid particles, this amount N of adsorbed molecules is usually measured in number of adsorbed molecules per unit of solid surface area, $[\mathrm{m}^{-2}]$.

The law of the evaluation of the number of the molecules on the solid surface, N, can be written as [17]

$$\frac{\partial N}{\partial t} = R_{\mathrm{ads}} - R_{\mathrm{des}}, \tag{1}$$

where R_{ads} and R_{des} are the adsorption and desorption rates, respectively. If we assume that the adsorption-desorption process equilibrates on a faster time scale compared to that of the gas transport, then the adsorption and desorption are always in equilibrium, *i.e.* $R_{\text{ads}} = R_{\text{des}}$.

To estimate the number of gas molecules hitting the surface per second, we recall the kinetic theory of ideal gases [18]. In textbooks of physical chemistry [18], [16] the rate of effusion of an ideal gas through a small hole, which can be associated to the adsorption rate, is given by

$$R_{\text{ads}} = \frac{\sigma A p}{\sqrt{2\pi m k_{\text{B}} T}} N_a, \tag{2}$$

where A is the cross-sectional area of one binding site. It can be estimated as a molecular cross-section area, which is of the order of Å^2, σ is the adsorption probability. Additionally, p is the gas pressure (the partial pressure is used instead of pressure, in the case of gas mixture), k_{B} is the Boltzmann constant, m is the molecular mass, T is the temperature, N_a is the number of the site available for adsorption per unit surface area. When the maximal adsorption capacity of a solid surface, N_{max}, *i.e.* the total number of available adsorption sites per unit of area, is non infinite number, then the number of the sites available for adsorption could be written as:

$$N_a = N_{max} - N. \tag{3}$$

If we assume that each molecule that hits the surface sticks to it with a probability σ, expression (2), then we can define the adsorption coefficient as:

$$K_{\text{ads}} = \frac{\sigma A}{\sqrt{2\pi m k_{\text{B}} T}}. \tag{4}$$

On the other hand, the desorption rate is proportional to the number of the molecules on the solid surface, N, and it is expressed as:

$$R_{\text{des}} = K_{\text{des}} N, \tag{5}$$

where the desorption constant, K_{des} is calculated from:

$$K_{\text{des}} = \nu \exp\left(-\frac{Q}{\mathcal{R}_g T}\right), \tag{6}$$

here ν is the oscillation frequency, $\nu = 1/\tau_0$, τ_0 is the adsorption time, $\mathcal{R}_g$=8.314 [J·K^{-1}mol^{-1}] is universal gas constant and Q is the heat of adsorption [18], [16].

If the reaction proceeds so slowly that it does not have time to come to local chemical equilibrium, then the kinetics of adsorption-desorption is not instantaneous and requires a dynamic rate law for its description, as Eq. (1). Therefore, the rate of adsorption depends on both quantities, n and N, being n the gas number density, which is related to the pressure through equation of state, $n = p/(k_{\text{B}}T)$. We could reason, for example, that the adsorption rate

should increase as the number density n of solute increases but, as more and more chemical is adsorbed, the ability of the solid to adsorb additional chemical decreases. The simplest model with these characteristics is:

$$\frac{\partial N}{\partial t} = K_{ads}(N_{max} - N)nk_{\mathrm{B}}T - K_{des}N. \tag{7}$$

When the simultaneous adsorption and desorption of different species is considered, the changes in the surface number density for species i, N_i, is expressed as

$$\frac{\partial N_i}{\partial t} = K_{ads,i}n_i k_{\mathrm{B}}T\left(N_{max} - \sum_{j=1}^{l} N_j\right) - K_{des,i}N_i, \qquad i = 1, l, \tag{8}$$

l is the total number of pollution species, excluding the carrier gas. Since the flow of carrier gas is constant, we assume that its adsorption and desorption rates are in equilibrium and do not change the total number of available adsorption site per unit of surface area. In the following we assume that the surface covered by the carrier gas molecules is already accounted in the evaluation of N_{max} and it does not change during the chromatographic analysis.

Some authors have studied adsorption and desorption phenomenon of the BTEX molecules on different adsorbents [19], [20]. However, there is no available data relative to coefficients of adsorption and desorption of BTEX molecules on the stationary phase of this particular column.

2.2. Model of carrier gas flow in a column

The flow of a carrier gas through the chromatography column transports a very small quantity (order of tens of ppb) of molecules of BTEX. Since the amount of BTEX is indeed very small, these molecules cannot perturb the dynamics of the carrier gas flow. Therefore, this flow is modeled from Navier-Stokes equations applied to compressible gas, flowing through a circular tube driven by a constant static pressure difference. The gas properties are supposed to be those of carrier gas. Besides, the gas flow inside the GC column can be considered as isothermal, since the temperature is set by the operator and maintained at a constant value during an analysis. In addition, a typical GC column have very small radius to length ratio and the gas velocity along the column is much higher than the radial velocity. These properties allow us to reduce the system of compressible Navier Stokes equations to the Stokes equation, see Refs. [21], [22].

The Stokes equation completed by the non-slip boundary condition on the column surface and zero velocity gradient on the column axe of symmetry was solved analytically in Ref. [22]. The complete expression of the gas velocity u parallel to the column axis, denoted in following as x, reads

$$u(r, x) = -\frac{R^2}{4\mu}\frac{dp}{dx}\left(1 - \frac{r^2}{R^2}\right), \tag{9}$$

where r is the radial axis and R is the column radius. The viscosity coefficient μ is calculated taking into account its temperature dependence in the form [23]:

$$\mu = \mu_{ref} \left(\frac{T}{T_{ref}} \right)^{\omega}. \tag{10}$$

In the previous expression μ_{ref} is the viscosity at the reference temperature $T_{ref} = 273.15$ [K], and ω is the viscosity index [23].

The dependency of the velocity from r variable can be eliminated by averaging over the column cross-section:

$$\overline{u}(x) = \frac{1}{\pi R^2} \int_0^R \int_0^{2\pi} u(r,x) r dr d\varphi = \frac{2}{R^2} \int_0^R u(r,x) r dr = -\frac{R^2}{8\mu} \frac{dp}{dx}. \tag{11}$$

The mass flow rate through a column cross section, $A_{\rm c}$, is calculated from the following expression:

$$\dot{M} = \pi R^2 \rho \overline{u}(x) = A_c \rho \overline{u}(x) = \int_{A_{\rm c}} \rho u(r,x) dA_{\rm c} = -\frac{\pi R^4 p}{8\mu \mathcal{R} T} \frac{dp}{dx}. \tag{12}$$

In the previous equation, ρ is the gas density, $\mathcal{R}$ is the specific gas constant, $\mathcal{R} = \mathcal{R}_g / \mathcal{M}$, and $\mathcal{M}$ is the gas molar mass. By integrating Eq. (12) from 0 to x, the pressure distribution along the column can be calculated from:

$$p(x) = p_{in} \sqrt{1 - \frac{x}{L}(1 - \mathcal{P}^2)}, \qquad \mathcal{P} = \frac{p_{out}}{p_{in}} \tag{13}$$

and the pressure gradient along the column by:

$$\frac{dp(x)}{dx} = -\frac{p_{in}\left(1 - \mathcal{P}^2\right)}{2L} \left(1 - \frac{x}{L}\left(1 - \mathcal{P}^2\right) \right)^{-1/2}. \tag{14}$$

As previously mentioned, the flow is isothermal. Thus, if the pressure distribution, Eq. (13), is known, the number density, n, or density, ρ, distributions can also be calculated from the equation of state.

Finally, to calculate the carrier gas velocity distribution along the GC column, (9), (14), the geometrical parameters of the column, the pressures at the column ends and the gas nature must be specified. One example of the velocity and pressure profiles along the column is provided in Appendix A.

2.3. Model of multi-species flow in a GC column

To describe the transport of a gas species inside the CG column we use the continuity equation of a species i, Ref. [24], called also the convection-diffusion equation. This equation is expressed in cylindrical coordinates as:

$$\frac{\partial n_i}{\partial t} + \frac{\partial (n_i u)}{\partial x} = \frac{1}{r} \left(\frac{\partial}{\partial r} \left(r \mathscr{D}_{iN_2} \frac{\partial n_i}{\partial r} \right) \right) + \frac{\partial}{\partial x} \left(\mathscr{D}_{iN_2} \frac{\partial n_i}{\partial x} \right), \tag{15}$$

where $n_i = n_i(t, r, x)$ is number density of species i, which is supposed here to be also the column cross-section coordinate, r, dependent. The carrier gas velocity, $u(r, x)$, depends also from two r and x coordinates and is given by Eqs. (9), (14). As it was done for the carrier gas transport modeling, in Section 2.2, we neglected the radial component of macroscopic velocity compared to the longitudinal one. In addition, the terms of the thermo-diffusion are also neglected and only mass diffusion is considered. As the concentration of the analyzed species in the mixture is very small, of the order of several ppb, compared to that of the carrier gas, only a binary diffusion coefficient is considered. Therefore the effect of the collisions among all the other species is neglected. Therefore, here $\mathscr{D}_{iN_2}$ is the binary diffusion coefficient of a molecule of BTEX (i index) with the carrier gas, N_2 (N_2 index), see Appendix B for the details of binary diffusion coefficient calculation and its typical values.

Equation (15) can be averaged over the column cross-section, introducing the averaged over cross-section number density as

$$\overline{n_i}(t, x) = \frac{2}{R^2} \int_0^R n_i(t, r, x) r dr. \tag{16}$$

In addition, we use the average over the cross-section velocity $\overline{u}$ according to Eq. (11). Besides, the integral over the cross-section for the first term of the right-hand-side of Eq. (15) can be calculated explicitly, therefore we obtain:

$$\frac{\partial \overline{n_i}}{\partial t} + \frac{(\partial \overline{n_i u})}{\partial x} = -\frac{2}{R} \mathscr{D}_{iN_2} \frac{\partial n_{\mathrm{i}}}{\partial r}\Big|_{r=R} + \frac{\partial}{\partial x}\left(\mathscr{D}_{iN_2} \frac{\partial \overline{n_i}}{\partial x} \right). \tag{17}$$

It is important to note that several terms were neglected during this averaging procedure, but they are considered not essential for the presented analysis. The first term in the right-hand side of previous equation represents the mass flux from (or to) the column surface. This flux can be evaluated using the adsorption-desorption fluxes balance as

$$-\frac{2}{R} \mathscr{D}_{iN_2} \frac{\partial n_{\mathrm{i}}}{\partial r}\Big|_{r=R} = \frac{2}{R} \left(R_{\mathrm{ads_i}} - R_{\mathrm{des_i}} \right). \tag{18}$$

This condition is a balance between diffusive flux in the normal direction to the surface and net adsorption-desorption rate, so condition (18) allows to evaluate the molecular flux on the column surface, $r = R$, in Eq. (17). In addition, this adsorption-desorption flux balance can be calculated via Eq. (7). Thereby, the concentration of a species i can be obtained from:

$$\frac{\partial n_i}{\partial t} + \frac{(\partial n_i u)}{\partial x} = -\frac{2}{R} \frac{\partial N_i}{\partial t} + \frac{\partial}{\partial x}\left(\mathscr{D}_{iN_2} \frac{\partial n_i}{\partial x} \right). \tag{19}$$

For simplicity we omitted the "bar" over the velocity and concentration in Eq. (19). The term $\partial N_i / \partial t$ quantifies the evolution in time of the number of adsorbed molecules and represents the balance of the adsorption-desorption fluxes, $R_{\mathrm{ads_i}} - R_{\mathrm{des_i}}$. The explicit expressions for the adsorption and desorption fluxes

depend on the adsorption-desorption model used in the analysis. The evaluation of the arial concentration of the adsorbed molecules in time is calculated here from Eq. (8). Therefore, in the following we solve numerically the system of two equations for each species i ($i = 1, l$):

$$\frac{\partial n_i}{\partial t} + \frac{\partial (n_i u)}{\partial x} = -\frac{2}{R}\frac{\partial N_i}{\partial t} + \frac{\partial}{\partial x}\left(\mathscr{D}_{iN_2}\frac{\partial n_i}{\partial x}\right),$$
$$\frac{\partial N_i}{\partial t} = K_{\mathrm{ads_i}}\left(N_{max} - \sum_{j=1}^{l} N_j\right) n_i k_{\mathrm{B}} T - K_{\mathrm{des_i}} N_i. \tag{20}$$

It should be mentioned that the second equation of system (20) requires the information about the part of surface covered by other pollutant molecules, so this system has to be solved simultaneously with the analogous systems for other species.

The initial and boundary conditions have to be specified for the system (20). We can assume that initially there is not any species in the CG column

$$n_i(0, x) = 0, \qquad 0 < x < L, \tag{21}$$

and that the column surface is bare (non pollutant molecule adsorbed):

$$N_i(0, x) = 0, \qquad 0 < x < L. \tag{22}$$

The determination of the maximum of adsorption capacity, N_{max} value, is provided in Section 5.2.

The composition of gas at inlet is known (see Section 5.1) and the pollutant is injected during a controlled time, thus the associated inlet boundary condition is simply:

$$n_i(t, 0) = n_{\mathrm{inj}}, \qquad 0 \leq t \leq t_{\mathrm{inj}}, \tag{23}$$

3. Experimental Approach

In order to validate the mathematical model and its numerical implementation we acquired experimental data using the facilities and devices provided by In'Air Solutions and ICPEES. The experimental setup consists of one gas cylinder of pure nitrogen, one gas cylinder of 100 ppb of each species of the BTEX mixture, 600 ppb in total. A flow regulator that controls the flow of BTEX mixture and a pressure regulator that controls the pressure at the inlet of the column and therefore the velocity of the carrier gas, N_2, through the chromatography column. A 6-port valve in combination with a sampling loop, sends the right volume of mixture towards the column in a two steps process. That way, 200 μL of 100 ppb of each species in the BTEX mixture is accurately injected into the GC column. When the injection is started the software starts recording the signal from the PhotoIonization Detector (PID).

The characteristics of all the components previously introduced are presented in Table 2, while a schematic representation of experimental configuration is

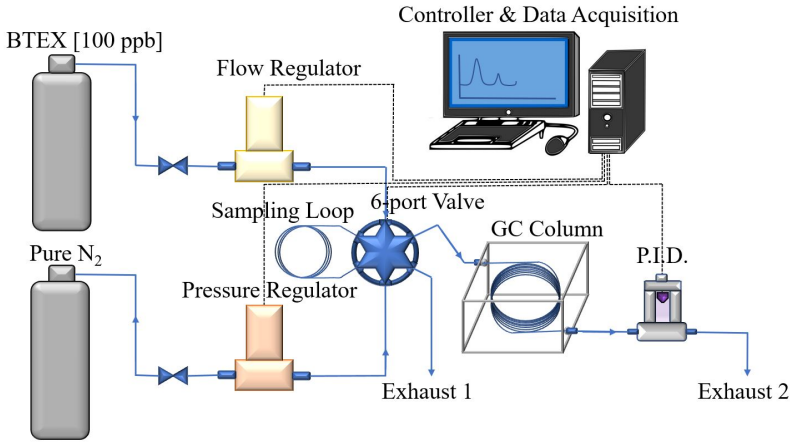

Figure 2: Scheme of the BTEX analyzing system setup in the analysis mode.

displayed in Fig. 2. The two components that affect more directly the BTEX molecules separation and detection are the GC column and the PhotoIonization detector. The GC column is a 20-m long capillary column with 0.18 mm of internal diameter, RXi-624 stationary phase, 1 μm film thickness (Restek, Bellefonte, PA, USA). Its coating is a combination of 95% PDMS + 5% cyanopropyl phenyl. This kind of coating is slightly polar and was selected among others based on experimental data. The detection unit is an eVx Blue mini PhotoIonization Detector (PID) (Baseline MOCON, Lyons, CO, USA) equipped with a high performance 10.6eV ultra-violet lamp which has different sensitivities for each compound. Different sensitivities means also different response factors. The BTEX analyzer do not incorporate any sort of purge, trap, headspace of precconcentrator that can influence the flow. More details about the GC system and BTEX analyzer can be obtained in Refs. [10], [11], [25].

Characteristics of the components	
mass flow controllers	Bronkhorst (Montigny les Cormeilles)
mini-diaphragm air pump	Schwarzer 270 EC
solenoid 6 ports valve	Takasago MTV-6LL-N32UF-1
sampling loop	CHEMINERT, 200μL
column	Rxt-624 (Length 20m/ID 0.18mm/df 1.00μm)
stationary phase	RXi-624 MS − 1μm film thickness
oven temperature controller	Farnell Cal 3300

Table 2: Models and brands of the components used in the experimental apparatus

4. Experimental conditions

A series of the measurements are carried out, varying two parameters: the pressure imposed in the inlet of the column, p_{in}, (p_{out} fixed at atmospheric pressure) and temperature of the column. These nine operating conditions are presented in Table 3.

Below we provide the details on the "standard case", case E, see Table 4. For the case E the pressures at the inlet and outlet sections of the GC column are fixed to 4bar and 1bar, respectively, with the constant temperature equal to 65°C. The volumetric flow rate is measured on both inlet and outlet sections of the column, see Table 4. From these flow rates, the carrier gas velocities in the inlet and outlet cross-sections of the column are calculated. Obviously, as $\Delta p/p > 1$, the variations of the gas density with position are significant and the volumetric flow rate (velocity) varies along the column. For case E, inlet velocity is 0.4 m/s while outlet one is 1.64 m/s, see also Fig. A.8 in Appendix A. By using the outlet velocity the Reynolds number is estimated to be less then 10, so the flow inside column is essentially laminar.

Operating Conditions	p_{in} [bar]	T [°C]
A	3	55
B	4	55
C	5	55
D	3	65
E standard	4	65
F	5	65
G	3	75
H	4	75
I	5	75

Table 3: Experimental operating conditions

5. Numerical implementation

As the BTEX concentration is very low, dilute approximation is chosen for modeling the advection, and only binary diffusion (pollutant in the carrier gas) is considered. On the other hand, as the species adsorb simultaneously on the solid, the available adsorption sites for a given species at a time moment depend on the already adsorbed amount of all species. Finally, we introduce the specific surface (m^2/m^3) of the solid, 2/R, to express all molecule density per unit of fluid volume, *i.e.* $N_i^{\text{V}} = 2N_i/R$, so N_i^{V} is now the number of molecules on the column surface per unit of volume. Thus, the system (20) becomes the following

Characteristics of the flow for E case	
carrier gas	Nitrogen
column length	$L = 20\text{m}$
column radius	$R = 0.09\text{mm}$
inlet pressure	$p_{in} = 4\text{bar}$
inlet volumetric flow rate	$Q_{in} = 0.625\text{ml/min}$
inlet gas density	$\rho_{in} = 3.98\text{kg/m}^3$
inlet flow velocity rate	$u_{in} = 0.41\text{m/s}$
outlet pressure	$p_{out} = 1\text{bar}$
outlet volumetric flow rate	$Q_{out} = 2.5\text{ml/min}$
outlet gas density	$\rho_{out} = 0.99\text{kg/m}^3$
outlet flow velocity rate	$u_{out} = 1.64\text{m/s}$
temperature	$T = 65^\circ\text{C}$
injection time	$t_{inj} = 4\text{s}$
initial BTEX concentration	$c_{inj} = 100\text{ppb}$
volume of sampling loop	$V_s = 200\mu\text{l}$

Table 4: Characteristics of the flow of carrier gas for the standard condition, case E.

one (all equations are solved simultaneously):

$$\begin{aligned}
&\frac{\partial n_i}{\partial t} + \frac{\partial (n_i u)}{\partial x} = -\frac{\partial N_i^{\mathrm{V}}}{\partial t} + \frac{\partial}{\partial x}\left(\mathscr{D}_{iN_2}\frac{\partial n_i}{\partial x}\right), \\
&\frac{\partial N_i^{\mathrm{V}}}{\partial t} = K_{\mathrm{ads_i}}\left(N_{\mathrm{max}}^{\mathrm{V}} - \sum_{j=1}^{l} N_j^{\mathrm{V}}\right) n_i k_{\mathrm{B}} T - K_{\mathrm{des_i}} N_i^{\mathrm{V}}.
\end{aligned} \tag{24}$$

To numerically solve the system (24) we used a simple Finite Volume approach, with a spacial discretization step, Δx, of 1mm and a temporal one, Δt, of 0.5 ms, so the volume of each numerical cell, $V_{\mathrm{cell}} = \pi R^2 \Delta x$, is equal to $2.49 \cdot 10^{-11}$ m^3.

For convenience we choose to express both densities, n_i and N_i^{V} in number of molecules per computational cell, by multiplying both equations of system (24) by the volume of the computational cell, V_{cell}. Now $\mathfrak{n}$ is the number of molecules of species i in one millimeter of the column in gas phase, while $\mathfrak{N}_i$ is the number of molecules of species i adsorbed in one millimeter of the stationary phase of the column, so the system (24) becomes

$$\begin{aligned}
&\frac{\partial \mathfrak{n}_i}{\partial t} + \frac{\partial (\mathfrak{n}_i u)}{\partial x} = -\frac{\partial \mathfrak{N}_i}{\partial t} + \frac{\partial}{\partial x}\left(\mathscr{D}_{iN_2}\frac{\partial \mathfrak{n}_i}{\partial x}\right), \\
&\frac{\partial \mathfrak{N}_i}{\partial t} = K_{\mathrm{ads_i}}^{*}\left(\mathfrak{N}_{max} - \sum_{j=1}^{l} \mathfrak{N}_j\right) \mathfrak{n}_i k_{\mathrm{B}} T - K_{\mathrm{des_i}} \mathfrak{N}_i.
\end{aligned} \tag{25}$$

In the second equation $K_{\mathrm{ads_i}}^{*}$ is equal to $K_{\mathrm{ads_i}}/V_{\mathrm{cell}}$. The system (25) represents simultaneously the variation of number of molecules of species i in each numer-

ical cell, or in other words, the variation in the number of adsorbed, desorbed and transported molecules of species i per millimeter of the column.

The initial conditions (injection of the BTEX species) and the boundary conditions (the maximum site available for adsorption on the column surface) need to be estimated.

5.1. Calculation sampling loop

The sampling loop has a length of 0.25 m and an internal volume of 200 μL. It is filled with a homogeneous mixture of BTEX at atmospheric pressure. Nevertheless, when the six-port valve is switched to the second position the pressure suddenly increases up to 4 bars. This increase is generated by the stream of N_2 coming from the second tubing line. The nitrogen compresses the initial content of the sampling loop in a space 4 times smaller, 50 μL, and therefore increases the concentration by a factor of 4. Thus, even though the injection time needed to transport the content of the sampling loop into the column is 16 seconds, the first 4 seconds contains the large majority of the BTEX molecules. The simulation of the injection in the GC-column were performed taking this fact into consideration.

The experimental chromatograms were obtained when injecting an initial concentration of 100 ppb of each species. Considering that the temperature of the column is T = 338 K, and the pressure at the inlet is 4 bars we can transform the concentration from ppb to molecules per cubic meter using the well-known ideal gas law

$$pV = \mathcal{N}\mathcal{R}_g T, \tag{26}$$

where $\mathcal{N}$ is amount of substance, [mol], V is the gas volume [m^3]. Under our injection condition, from Eq. (26) we calculate $\mathcal{N}/V$ equal to 142.33 mol·m^{-3}. To obtain the initial concentration in molecules per cubic meter we use the formula

$$n_{\text{inj}} = \frac{\mathcal{N}}{V} c_{\text{inj}} \mathcal{N}_A, \tag{27}$$

where $\mathcal{N}_A$=6.022·10^{23} [mol^{-1}] is the Avogadro number. From Eq. (27) we calculate n_{inj}=8.57·10^{18} [molecules·m^{-3}]. Thus, the inlet concentration is fixed at $\mathfrak{n}_i = 2.134 \cdot 10^8$ molecule/mm during the first 4 second.

5.2. Calculation of the number of free sites

The RXt-624 column is coated with a product which consists in 95% PDMS and 5% cyanopropyl phenyl. The total available for adsorption specific surface area of this coated layer is unknown, however we can get an approximation using published data from the literature. The authors of Ref. [26] studied a similar PDMS sample and they obtained a specific area of 832 $m^2 \cdot g^{-1}$ and a density of 1.095 g·cm^{-3}. Our column is 20 m long, has an internal radius of 90 μm and a coating thickness of 1 μm resulting in a total volume of coating of $1.13 \cdot 10^{-2}$ mL or an equivalent mass of $1.24 \cdot 10^{-2}$ g. If we multiply this mass by the

specific area, we obtain the available surface of 10.3 m^2. We can estimate the effective surface of each molecules using their diameter, see Table 1. However, six BTEX molecules can adsorb to the surface, so we use the average over all six molecules radius, equal to $6.23{\cdot}10^{-10}$m. Assuming a monolayer of adsorption in accordance to the Langmuir theory [16], [15], and identifying a surface needed to adsorb one molecule as a square of $6.23 \cdot 10^{-10}$m of side, we obtain a total number of free places for "an average BTEX molecule", of $N^{\mathrm{V}}_{\max} = 5.23 \cdot 10^{25}$ in the whole column and $\mathfrak{N}_{\max} = 1.302 \cdot 10^{15}$ in a computational cell. This last value is several orders of magnitude higher than the number of molecules that we are injecting in the column. Therefore, even if the error of this assumption is of one or two orders of magnitude it would make no difference in the overall results.

5.3. Numerical scheme

The system (25) was splited in two parts: the advection-diffusion and the adsorption-desorption one. At each time step we first solve the advection-diffusion part using a simple explicit upwind scheme (28) then add the contribution of the adsorption-desorption (30) - (32).

The numerical scheme for the advection-diffusion part is displayed here

$$\begin{aligned}(\mathfrak{n}_i)^*_k = (\mathfrak{n}_i)^j_k - \Delta t/\Delta x \left((\mathfrak{n}_i u)^j_k - (\mathfrak{n}_i u)^j_{k-1}\right) + \\ \Delta t/(\Delta x^2)\left(D^j_{k+1/2}\left[(\mathfrak{n}_i)^j_{k+1} - (\mathfrak{n}_i)^j_k\right] - D^j_{k-1/2}\left[(\mathfrak{n}_i)^j_k - (\mathfrak{n}_i)^j_{k-1}\right]\right), \quad k = 1, N_{\mathrm{L}} - 1.\end{aligned} \tag{28}$$

In previous equation, k index denotes the point k of the grid in physical space (along the column), j index denotes the time space, $*$ superscript indicates intermediate results during a time step, $D^j_{k\pm1/2} = 0.5\left((\mathscr{D}_{iN_2})^j_k + (\mathscr{D}_{iN_2})^j_{k\pm1}\right)$.

To approximate the reaction equation the number of free sites available for adsorption is introduced as $(\mathfrak{N}_{\mathrm{free}})^j_k = (\mathfrak{N}_{\max})_k - \sum_{q=1}^{l}(\mathfrak{N}_q)^j_k$, so the adsorption and desorption terms are approximated as following

$$(R_{\mathrm{ads_i}})^j_k = K_{\mathrm{ads_i}}(\mathfrak{N}_{\mathrm{free}})^j_k(\mathfrak{n}_i)^*_k k_{\mathrm{B}}T, \qquad (R_{\mathrm{des_i}})^j_k = \quad K_{\mathrm{des_i}}(\mathfrak{N}_i)^j_k. \tag{29}$$

Then the update of all parameters at the new time step is carried out, for the number of molecules in the gas phase

$$(\mathfrak{n}_i)^{j+1}_k = (\mathfrak{n}_i)^*_k - \Delta t\left((R_{\mathrm{ads_i}})^j_k - (R_{\mathrm{des_i}})^j_k\right), \tag{30}$$

for the number of adsorbed molecules

$$(\mathfrak{N}_i)^{j+1}_k = (\mathfrak{N}_i)^j_k + \Delta t\left((R_{\mathrm{ads_i}})^j_k - (R_{\mathrm{des_i}})^j_k\right) \tag{31}$$

and finally for the free places available for adsorption considering the balance of all six species:

$$(\mathfrak{N}_{\mathrm{free}})^{j+1}_k = (\mathfrak{N}_{\mathrm{free}})^j_k - \Delta t\sum_{q=1}^{l}\left((R_{\mathrm{ads_q}})^j_k - (R_{\mathrm{des_q}})^j_k\right). \tag{32}$$

The last relation ensure the conservation of number of particles during one time step. The described numerical procedure was reproduced up to the injected molecules left the column.

5.4. Adsorption and desorption constants

When it comes to the numerical implementation, model input parameters and equations of state are not easily available. This happens not only for this particular combination of stationary phase and mobile phase, but also for most of the analysis in pharmaceutical, biochemical, environmental and general gas chromatography. Therefore, the constants of adsorption and desorption, K_{ads} and K_{des}, were obtained following an iterative process using all the measured retention time values for all compounds.

6. Results

In this Section, first the chromatograms of BTEX compounds obtained from nine experiments for different operating conditions, Table 3, are presented and analyzed. After that, based on the chromatogram obtained from the experiment under standard operating condition, case E, the adsorption and desorption coefficients, K_{ads}, (4), and K_{des}, (6), of all the BTEX compounds are calibrated. Then, the numerical simulations are carried out for five from nine available operating conditions and the numerical results reproducing the variation of the concentration of all BTEX species in time along the column are compared to the experimental results.

6.1. Experimental results

The series of the experimental measurements are carried out, by varying two parameters: the pressure imposed in the inlet of the column, p_{in}, and temperature of the column, T, see Table 3. The injection condition remains the same, *i.e.* the volume of 200 μL (at 4 atm and room temperature) with the injected concentration of BTEX of 100 ppb.

The experimental chromatograms are presented in Figure 3. The tendencies of the graphs are clearly mark. The separation process is longer when lower inlet pressures are used while it takes less time for higher temperatures. In other words, the retention time of each compound tend to increase by using lower pressures and temperatures. The lower the inlet pressure, the slower the flow inside the column and therefore the longer the average time of the molecules to leave the column. On the other hand, the lower is the temperature, the lower is the kinetic energy of the molecules and the longer the average interactions between the two phases through of adsorption and desorption processes.

When it comes to a commercial application, a balance is needed between the chromatogram resolution and the time used for the process. If the separation process of every chromatogram last too long, it does not match many of the requirements needed in the monitoring process. Many of which require continuous monitoring and a good time resolution to correlate the sources of pollution

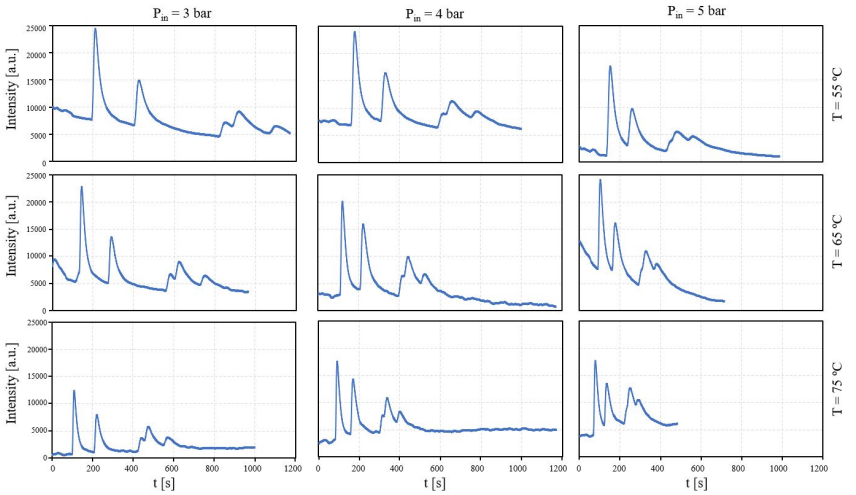

Figure 3: Chromatograms of BTEX separated inside the column for nine different operating conditions, see Table 3.

with the concentrations present in the air. However, if the separation process is too quick, the retention times of some of the compounds are too similar to each other and they may leave the column too close. Then, the compounds become coleluted and their peaks become overlapped inducing larger quantification errors of those species concentrations. Taking these facts into consideration, the chromatogram at 4 bar of inlet pressure and 65°C of temperature was taken as the standard one, (case E), being these conditions recommended by In'Air Solutions for the optimal separation of BTEX.

Some of the experimental chromatograms exhibited baseline drift, which happened due to the lack of stability in the PID. In practice, the lamp becomes stable after 24 hours being on and some time for stabilization is also require when the temperature or flow rate is modified. Nevertheless, the baseline instability does not affect to the retention time in any way.

6.2. Comparison between experimental and numerical results

In Figure 4 the temporal evolution of the pollutants inside the column simulated using the previously described method is displayed at $p_{\text{in}} = 4$ bar and $T = 65°\text{C}$ (case E). At time of 5s all injected species are seen in form of a Guassian pick, while at t=20s the first separation effects are clearly present. At time 120s benzene left the column and it is quantified by the PID detector, while at t=510s last species, *i.e.* o-xylene, also went out from the column.

The number of molecules at the very end of the column for every moment of time is then multiplied, so by multiplying this value by the PID response factor, varying between 0.50 and 0.53, depending on the aromatic compound, we obtain the simulated chromatogram. This later is compared to the experimental one in Fig. 5 for the standard conditions (case E).

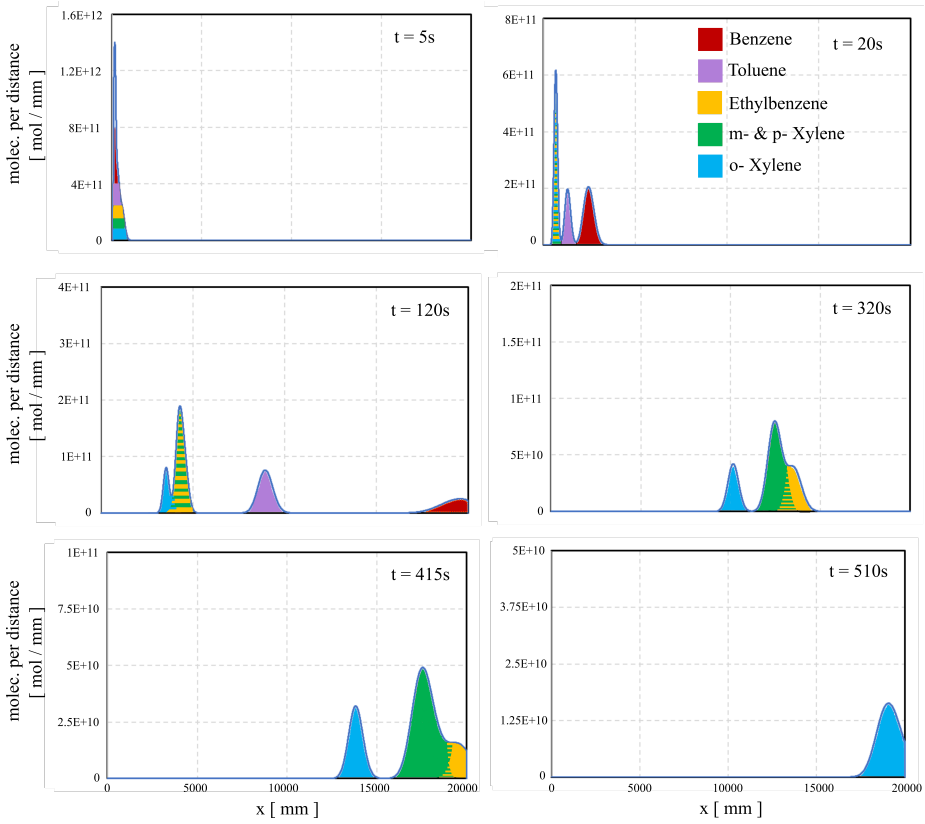

Figure 4: Temporal evolution of the pollutants inside the GC-Column, results of the numerical simulations in the standard conditions, case E.

There are some obvious differences between the two chromatograms displayed in Fig. 5. The numerical results show ideal chromatography peaks with a nice sharp symmetrical shape (Gaussian peak) and a flat baseline. In real conditions, the chromatographic peaks can deviate from this ideal. In Figures 3 and 5, the experimental peaks become asymmetric, broader, and sometimes the baseline slightly rises or decreases. This common shift away from a Gaussian peak is when the back half of the peak falls away. If the peak were split into two, vertically, the second half would be wider than the first half of the peak. This effect is known as peak tailing and is clearly observed in Figures 3 and 5 for all the experimental chromatograms. This effect can be originated due to several factors, namely contamination, column overloading, secondary silanol interactions, reversible chemical reactions or flow path disruption [27]. Indeed, determining the source, it is complex and often there are more than one. In our case we can neglect the column overloading, since concentrations 100 times higher have been successfully tested. Contamination can be neglected too, since

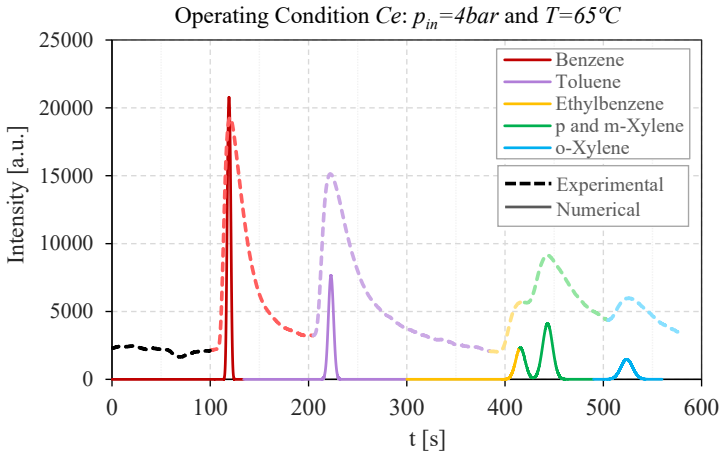

Figure 5: Chromatograms of BTEX separation for the standard conditions, case E, obtained from experiment (dashed line) and from numerical simulations (solid line).

no impurities are present in the commercial gas. Secondary, silanol interactions could contribute partially to the distortion of the experimental peaks even if this chromatography column is known to be very adapted to the BTEX separation [10], [11]. Ideally, this phenomenon could be also simulated by adding a secondary adsorption desorption reaction between the BTEX molecules and free silanol groups. However, activity coefficients and surface density of the silanol groups must be known.

Another reason for the peak tailing is a flow path disruption. In Section 5.1 we discussed the filling of the sampling loop and the effect of the compression of the sample. We suspect this is a source for peak tailing. When the injection is started the 6-port valve switches sending the 4-bars-pressure flow of nitrogen through the sampling loop. Even though, the core of the BTEX molecules is compressed in the front part of the sampling loop (first four seconds of injection) there is a part of the molecules that tend to spread back again to the initial part of the sampling loop. Therefore, and since the total time of injection is 20 seconds it might happened that the injection is already tailed before entering the GC-column. After all a troubleshooting process should be done experimentally to identify the source of the peak tailing. If the peak tailing comes effectively from a flow path disruption in the sampling loop or from a secondary silanol interactions it could be described mathematically and simulated either way.

The second and most important disagreement is the width of the peaks. The mini PID detector was chosen regarding its compact size for the GC portability issue. It is connected to the GC column outlet using a T-shape connector, so that the gas flow leaving the chromatography column does not cross directly the PID detection cell. In fact, the gas mixture diffuses from the GC column outlet to the detection cell through a permeation membrane, as illustrated in Fig. C.10. More precisely, pollutant molecules and carrier gas pass through the

permeation membrane and fill the cavity of the PID detection cell by passive diffusion due to concentration gradient. Therefore, the gas molecules require longer time to enter and leave the PID detection cell, increasing the width of the peaks. In addition, the filling process is faster than the emptying process because a rapid increase in the concentration gradient is expected when the pollutant enters into the PID detection cell, but the emptying process lasts longer since the more molecules leave the PID chamber the smaller the gradient becomes and the slower they abandon the PID detection cell. The geometry of the PID connection with the column is thus probably the main reason for the tailing effect, observed and discussed previously.

6.3. Predictions for other operating conditions

The prediction capability of the model can only be tested if the retention times are *a priori* unknown. Therefore, first two cases with the same operating temperature, 65°C, but different inlet pressure, equal to 3 and 5 bars, namely the cases D and F, see Table 3, are simulated, without using any information about measured retention time. Nonetheless, to do so, the K_{ads} and K_{des} constants were required. For standard case, case E, both constants are obtained by a fitting procedure using the measured retention time for each species. To simulate the cases D and F the same values of adsorption and desorption coefficients are kept, since these coefficients are pressure independent according to Eqs. (4) and (6).

The comparison between experimental and numerical results are presented in Fig. 6 (a) and (b), for the case D and F, performed at 3 and 5 bars, respectively, see Table 3. The comparison between the experimental and numerical curves shows that the general prediction is relatively good and the model allows to mimic the inlet column pressure changes. However, the intensity of the simulated peaks does not change with the inlet pressure changing, therefore the discrepancy with the simulations is larger for the lower pressures, where intensity of the measured signal is lower, especially for the heavier species.

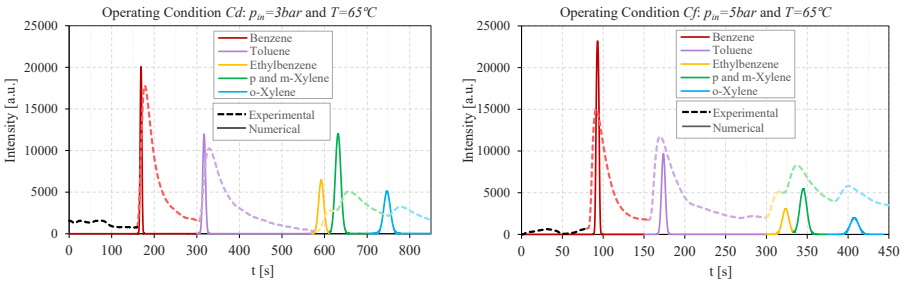

Figure 6: Chromatograms of BTEX species separation obtained from experiments (dashed line) and numerical simulation (solid line) for T = 65°C: (a) p_{in} = 3bar, case D, and (b) p_{in} = 5bar, case F.

The second, more complex comparison has been done between experimental and numerical results for two different working temperature, $T = 55°C$ and $75°C$, but using the same intet pressure of 4 bars. By analyzing the available analytical expressions for both adsorption and desorption coefficients, Eqs. (4) and (6), it is clear that they depend only on the temperature for the same species. By using the known temperature dependency of each coefficient from the temperature, *i.e.* $K_{\text{ads}} \propto 1/\sqrt{T}$ and $K_{\text{des}} \propto \exp(1/T)$ we adjusted the values of these coefficients for different temperature.

The comparisons between experimental and numerical results, for cases B and H, are shown on Fig. 7 (a) and (b), respectively. Here the influence of the temperature inside the column is evaluated. The same comments as for the previous results can be done: the numerical results do not allow to predict the intensity of peak when the conditions, here the temperature, change.

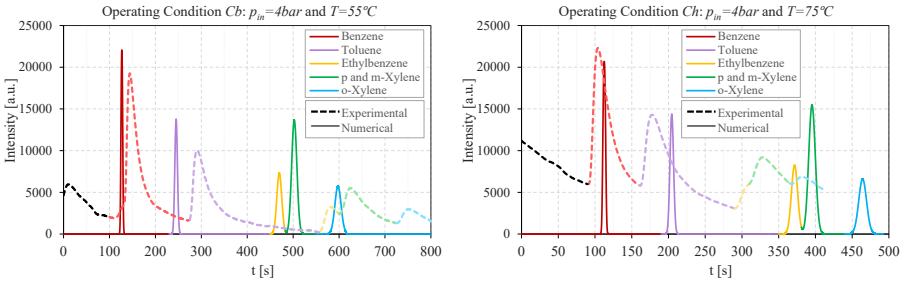

Figure 7: Chromatograms of BTEX species separation obtained from experiments and numerical simulations for inlet pressure 4 bar: (a) B case, $T = 55°C$, and (b) H case, $T = 75°C$.

The results of experimental and numerical retention times for the cases B, D, F and H, are presented in Table 5. The overall agreement between the experimental and numerical results is good. However, it is much better, of the order of 1.9-6.4%, for the cases D and F, where only inlet pressure changes. This agreement becomes less good, of the order of 8-24.4%, in the cases B and H, where the working temperature varies. This is due to the difficulties to model the temperature dependence of coefficients K_{ads} and K_{des}.

7. Conclusion

The mathematical model developed in this work has been proved valid for simulating gas-chromatographic interactions inside a gas-chromatographic column. The numerical evaluation based on this mathematical model resulted in accurate results that are in correlation to the experimental results. When either the column temperature is increased and, therefore, the intensity of the adsorption process is reduced, or the pressure at the inlet of the column is increased, the flow through the column is speeded up. Both conditions result in a reduction of the retention time as it was derived from the experimental and numerical

Condition	Species	$t_{R,exp}$ [s]	$t_{R,num}$ [s]	error [%]
B p_{in} = 4bar, T=55°C	Benzene	144.3	126.9	12.1
	Toluene	290.9	245.1	15.7
	Ethylbenzene	581.6	469.8	19.2
	m and p-Xylene	624.2	502.4	19.5
	o-Xylene	751.0	597.6	24.4
D p_{in} = 3bar, T=65°C	Benzene	177.9	168.9	5.1
	Toluene	328.9	317.0	3.6
	Ethylbenzene	612.8	592.2	3.4
	m and p-Xylene	675.0	631.7	6.4
	o-Xylene	780.8	746.6	4.4
F p_{in} = 5bar, T=65°C	Benzene	91.6	93.2	1.7
	Toluene	169.9	173.7	2.2
	Ethylbenzene	315.7	323.6	2.4
	m and p-Xylene	337.3	345.1	2.3
	o-Xylene	399.8	407.7	1.9
H p_{in} = 4bar, T=75°C	Benzene	104.0	113.1	8.0
	Toluene	177.8	205.0	13.2
	Ethylbenzene	313.0	372.1	15.9
	m and p-Xylene	328.7	395.9	17.0
	o-Xylene	382.2	464.8	17.8

Table 5: Retention time experimentally and numerically obtained for 4 operating conditions.

results. The major differences between the numerical and experimental results come from the shape of the chromatogram and the retention time. The peak tailing occurs mainly due to the experimental connection way between the GC column and the PID detector, inducing long diffusion time for gas to enter and to leave the detection cell. Besides, retention times variation can be associated with the approximations done in the calculation of K_{ads} and K_{des}.

Although the model presents some limitations, it can be a useful tool to perform the first analysis in the development and optimization of a chromatographic microcolumn, such as those fabricated by MEMS-techniques [28]. Since the activity coefficient models or values are not published for most of the potential gas chromatography simulations, there is a need of having at least one known experimental result. Further simulations must be done and must be correlated with experimental data for alternative analytes in order to be able to benefit from rigorous dynamic simulations using this model. Nonetheless, this approach has the potential to allow engineers and scientist to model and understand the chromatographic separation process for a wide range of applications, resulting in higher chromatographic separation. Additionally, it can be very useful at identifying optimal designs and improving profitability.

Appendix A. Example of macroscopic parameters profiles. Case E

Figure A.8 shows the profiles of averaged over the column cross-section carrier gas velocity (11) and pressure distribution (13) along the GC column for the standard case (case E) conditions, see Table 4. As it can be seen, the velocity increases along the column, according to expected. This happens because the pressure, and consequently the density, is higher at the inlet in comparison to the outlet of the column. Then, to satisfy the mass conservation along all the cross-sections of the tube, the velocity is lower for a higher density. Moreover, both velocity and pressure distributions are not linear.

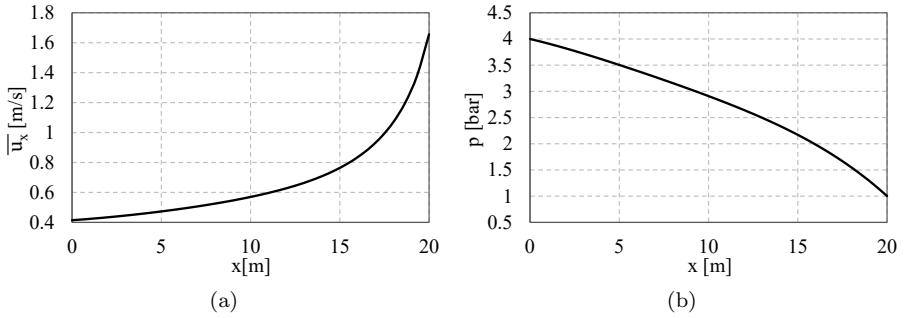

Figure A.8: Distribution of the carrier gas (a) velocity averaged over the cross-section and (b) pressure along the GC column.

Appendix B. Binary Diffusion Coefficient

In the column the gas mixture is flowing, but the concentration of the pollution is very low, so the binary diffusion coefficient of the carrier gas and each type of the pollution molecule has to be calculated. The binary diffusion coefficient of two species i and j, $\mathscr{D}_{ij}$, is obtained from Ref. [24]:

$$\mathscr{D}_{ij} = \frac{3}{8pd_m^2}\sqrt{\frac{(k_{\mathrm{B}}T)^3}{2\pi}\left(\frac{1}{m_i}+\frac{1}{m_j}\right)}, \tag{B.1}$$

where d_m is the mean collision cross-section diameter of species i and j:

$$d_m = \frac{1}{2}(d_i + d_j). \tag{B.2}$$

It is to underline that the Hard Sphere (HS) [24] model is used when calculated the binary diffusion coefficient. The values of the molecular diameter and molecular mass, needed for the calculation of binary mixture coefficients, are given in Table 1. The diffusion coefficient variation for all six species along the column is shown on Fig. B.9, where its strong variation can be observed.

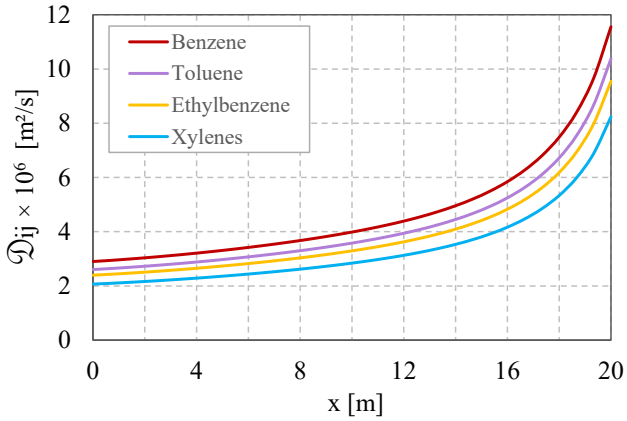

Figure B.9: Diffusion coefficient for some BTEX gases.

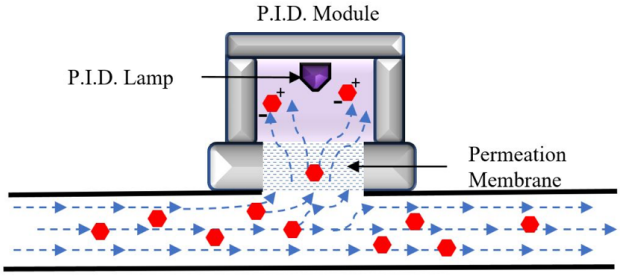

Figure C.10: Scheme of the PID detection system and its location in parallel to the flow at the outlet of the GC column. Red hexagons represent the BTEX molecules while the blue dashed arrows represent the flow direction of the carrier gas.

Appendix C. PID detection system

Scheme of the PID detection system is detailed in Fig. C.10.

Acknowledgements

The authors would like to acknowledge the financial support provided by the European Union network program H2020, MIGRATE project under Grant Agreement No.643095.

[1] D. C. Harris, Quantitative Chemical Analysis, 8th Edition, W.H. Freeman and Co., New York, NY, 2010.

[2] E. F. Barry, L. Robert, Columns for gas chromatography: performance and selection, John Wiley & Sons, 2007.

[3] E. V. Dose, Simulation of gas chromatographic retention and peak width using thermodynamic retention indexes, Analytical Chemistry 59, no. 19 (1987): 2414-2419 59 (19) (1987) 2414–2419.

[4] F. Aldaeus, Y. Thewalim, A. Colmsjö, Prediction of retention times of polycyclic aromatic hydrocarbons and n-alkanes in temperature-programmed gas chromatography, Analytical and bioanalytical chemistry 389 (3) (2007) 941–950.

[5] F. Aldaeus, Y. Thewalim, A. Colmsjö, Prediction of retention times and peak widths in temperature-programmed gas chromatography using the finite element method, Journal of Chromatography A 1216 (1) (2009) 134–139.

[6] K. Bryan, J. Harynuk, Prediction of gas chromatographic retention time via an additive thermodynamic model, Journal of Chromatography A 1217 (29) (2010) 4862–4867.

[7] A. Shukui, S. He, D. R. Worton, , A. H. Goldstein, Predictions of comprehensive two-dimensional gas chromatography separations from isothermal data, Journal of Chromatography A 1233 (2012) 147–151.

[8] S. Hazrati, R. Rostami, M. Farjaminezhad, M. Fazlzadeh, Preliminary assessment of BTEX concentrations in indoor air of residential buildings and atmospheric ambient air in Ardabil, Iran, Atmospheric Environment 132 (2016) 91–97. doi:10.1016/j.atmosenv.2016.02.042.
URL http://dx.doi.org/10.1016/j.atmosenv.2016.02.042

[9] R. A. Rinsky, Benzene and leukemia: An epidemiologic risk assessment, Environmental Health Perspectives 82 (1989) 189–191. doi:10.1289/ehp.8982189.

[10] R. Nasreddine, V. Person, C. A. Serra, C. Schoemaecker, Portable novel micro-device for BTEX real-time monitoring : Assessment during a field campaign in a low consumption energy junior high school classroom 126 (2016) 211–217. doi:10.1016/j.atmosenv.2015.11.005.

[11] I. Lara-Ibeas, A. Rodríguez-Cuevas, C. Andrikopoulou, V. Person, L. Baldas, S. Colin, S. Le Calvé, Sub-ppb level detection of BTEX gaseous mixtures with a compact prototype gc equipped with a preconcentration unit, Micromachines 187 (10).

[12] J. Lyu, L. Zhou, J. Shao, Z. Zhou, J. Gao, Y. Dong, Z. Wang, Tio_2 hollow heterophase junction with enhanced polluant adsorption, light harvesting, and charge separation for photocatalytic degradation of volatile organic compounds, Chemical Engineering Journal (123602).

[13] A. Yavarinasab, S. Janfaza, N. Tasnim, H. Tahmooressi, A. Dalili, Graphene/poly (methyl mathacrylate) elecrochemical impedance-transdued chemiresistor for detection of volatile organic compounds in aqueous medium, Analytica Chimica Acta 1109 (2020) 27–36.

[14] R. Hansen, H. Bruus, T. H. Callisen, O. Hassager, Transient convection, diffusion, and adsorption in surface-based biosensors, Langmuir 28 (2012) 7557–7563.

[15] I. Langmuir, The construction and fundamental properties of solid and liquids, J. Am. Chem. Soc. 38 (11) (1916) 2221–2295.

[16] H. J. Butt, K. Graf, M. Kappl, Physics and Chemistry of Interfaces, Wiley-VCH Verlag GmbH & Co. KGaA, Weinheim, Germany, 2003, Ch. Adsorption, pp. 177–205.

[17] T. Wolkenstein, Electron Theory of catalysis on Semiconductors, Pergamon. Oxford, 1963.

[18] D. D. Do, Adsobtion analysis: equilibria and kinetics, Vol. 2, Imperial College Press, Imperial College London SW7 2BT, 1998.

[19] Z. Zhao, X. Li, S. Huang, Q. Xia, Z. Li, Adsorption and Diffusion of Benzene on Chromium-Based Metal Organic Framework MIL-101 Synthesized by Microwave Irradiation, Industrial & Engineering Chemistry Research 50 (4) (2011) 2254–2261. doi:10.1021/ie101414n.
URL http://dx.doi.org/10.1021/ie101414n

[20] I. Lara-Ibeas, C. Megías-Sayago, A. Rodríguez-Cuevas, R. Ocampo-Torres, B. Louis, S. Colin, S. Le Calvé, Adsorbent screening for airbone btex análisis and removal, Journal of Environmental Chemical Engineering (2019) 103563.

[21] H. R. van den Berg, C. A. ten Seldam, P. S. van den Gulik, Compressible laminar flow, Journal o Fluid Mechanics 246 (1993) 1–20.

[22] I. A. Graur, J. G. Méolans, D. E. Zeitoun, Analytical and numerical description for isothermal gas flows in microchannels, Microfluid and Nanofluid 2 (2006) 64–77.

[23] G. A. Bird, Molecular Gas Dynamics and the Direct Simulation of Gas Flows, Oxford Science Publications, Oxford University Press Inc., New York, 1994.

[24] J. H. Ferziger, H. G. Kaper, Mathematical Theory of Transport Processes in Gases, North-Holland Publishing Company, Amsterdam, 1972.

[25] A. Rodríguez-Cuevas, I. Lara-Ibeas, A. Leprince, M. C. W. Wolf, S. Le Calv/'e, Easy-to-manufacture micro gas preconcentrator integrated in a portable gc for enhanced trace detection of btex, Sensors and Actuators B: Chemical (128690).

[26] Y. Ah Noh, S. Song, H. T. Kim, Fabrication and characterization of Aerogel-Polydimethyl Siloxane (PDMS) insulation film, Journal of Physics: Conference Series. IOP Publishing (2018) 012018.

[27] J. de Zeeuw, Ghost peaks in gas chromatography part i: The carrier gas and carrier gas lines, in: Guide to GC Column Selection and Optimizing Separations, Vol. 5, Separation Science, 2013.

[28] B. P. Regmi, M. Agah, Micro gas chromatography: An overview of critical components and their integration, Analytical Chemistry 90 (2018) 13133–13150.